ORIGINAL PAPER

Intermediates Arising from the Water–Gas Shift Reaction over Cu Surfaces: From UHV to Near Atmospheric Pressures

K. Mudiyanselage · S. D. Senanayake · P. J. Ramirez ·
S. Kundu · A. Baber · F. Yang · S. Agnoli · S. Axnanda ·
Z. Liu · J. Hrbek · J. Evans · J. A. Rodriguez · D. Stacchiola

Abstract The water–gas shift (WGS) reaction ($CO + H_2O \rightarrow CO_2 + H_2$) is a key process to the production of high purity H_2 from gas streams rich in CO. The identification of the WGS reaction mechanism and the probable stable intermediates is critical to design the catalyst structure, optimize composition and tune reaction kinetics/thermodynamics to achieve the optimum selectivity and activity. In this study, first the WGS reaction steps on Cu(111) have been studied using X-ray photoelectron spectroscopy (XPS) and infrared reflection absorption spectroscopy under ultra-high vacuum (UHV) conditions. Then the interactions of H_2O with CO on Cu(111) have been studied under elevated pressures (90 mTorr CO + 30 mTorr H_2O) at 300–575 K with ambient pressure XPS. Under UHV conditions, non-dissociative adsorption of H_2O on Cu(111) and Cu_2O/Cu(111) was observed. Whereas H_2O readily dissociates, by breaking the O–H bond on a chemisorbed O layer on Cu(111) to form OH species. Even though this OH interacts with adsorbed CO, it does not react to form any associative intermediate and simply desorbs as H_2O at 275 K under UHV conditions. At ambient pressures, no associative intermediates species, only CO and OH, were observed in the reaction of CO with H_2O although the catalytic production of H_2 can be detected under these conditions. Since intermediate species other than CO and OH were not observed on Cu(111) under reaction conditions, we concluded that the redox mechanism is the dominant WGS pathway on Cu(111). The coupling of Cu to an oxide, Cu–CeO_2 catalyst, or a carbide, Cu–TiC catalyst, favors an associative mechanism and produces a very large increase in the rate for the production of H_2 through the WGS.

Keywords Water–gas shift · Hydrogen production · Copper · Ceria · Titanium carbide

1 Introduction

The forward water–gas shift (WGS) reaction ($CO + H_2O \rightarrow CO_2 + H_2$) is a very important process and has a wide range of direct and indirect applications in industrial processes such as the purification of synthesis gas, synthesis of ammonia and alcohols and fuel cell related reactions. The industrial standard for this low temperature WGS reaction are typically copper based catalysts, composed of Cu/ZnO/Al_2O_3. In general, the Cu can be dispersed on oxide or carbide surfaces [1–3]. For metallic copper, the most energetically favored surface is the (111), and this surface serves as a good model system for the active Cu component in the high surface area Cu/ZnO/Al_2O_3 powder catalyst. To date many experimental and theoretical studies relating to the WGS reaction have been performed with the Cu(111) surface, and specifics relating to the mechanism and intermediates have been hotly

K. Mudiyanselage · S. D. Senanayake · S. Kundu · A. Baber ·
F. Yang · S. Agnoli · J. Hrbek · J. A. Rodriguez ·
D. Stacchiola (✉)
Chemistry Department, Brookhaven National Laboratory,
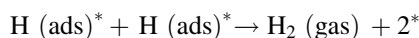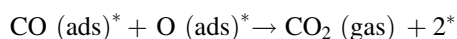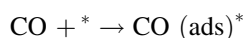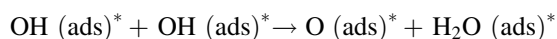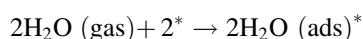Upton, NY 11973, USA
e-mail: djs@bnl.gov

J. A. Rodriguez
e-mail: rodrigez@bnl.gov

P. J. Ramirez · J. Evans
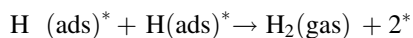Facultad de Ciencias, Universidad Central de Venezuela,
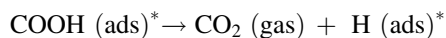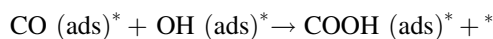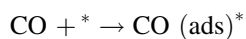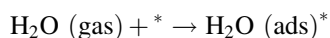Caracas 1020A, Venezuela

S. Axnanda · Z. Liu
The Advanced Light Source, Lawrence Berkeley National
Laboratory, Berkeley, CA 94720, USA

debated [1, 3–6] From these studies, mainly two mechanisms (redox and associative) have been considered as most probable for the WGS reaction over Cu based catalysts and are presented below:

1.1 Redox Mechanism

$$2H_2O \ (gas) + 2^* \rightarrow 2H_2O \ (ads)^*$$

$$2H_2O \ (ads)^* + 2^* \rightarrow 2OH \ (ads)^* + 2H \ (ads)^*$$

$$OH \ (ads)^* + OH \ (ads)^* \rightarrow O \ (ads)^* + H_2O \ (ads)^*$$

$$CO + ^* \rightarrow CO \ (ads)^*$$

$$CO \ (ads)^* + O \ (ads)^* \rightarrow CO_2 \ (gas) + 2^*$$

$$H \ (ads)^* + H \ (ads)^* \rightarrow H_2 \ (gas) + 2^*$$

1.2 Associative Mechanism

$$H_2O \ (gas) + ^* \rightarrow H_2O \ (ads)^*$$

$$H_2O \ (ads)^* + ^* \rightarrow OH \ (ads)^* + H \ (ads)^*$$

$$CO + ^* \rightarrow CO \ (ads)^*$$

$$CO \ (ads)^* + OH \ (ads)^* \rightarrow COOH \ (ads)^* + ^*$$

$$COOH \ (ads)^* \rightarrow CO_2 \ (gas) + H \ (ads)^*$$

$$H \ (ads)^* + H(ads)^* \rightarrow H_2(gas) + 2^*$$

In the redox mechanism, CO reacts with O, which is derived from the dissociation of H_2O, to form CO_2. The dissociation of H_2O also leads to the production of H_2 by the recombination of adsorbed H. In the associative process, a stable COOH intermediate species must precede the formation of H_2 and CO_2. It has been proposed with some

controversy that the predominant intermediate species for this reaction is either a surface bound formate (HCOO) or a *carbonate* (CO_3) species. In addition, recent theoretical calculations also suggest the possibility of a *carboxyl* (COOH) [5, 7] intermediate but this species remains experimentally elusive and difficult to detect. Despite these many studies [1–6], the detailed mechanism of the WGS reaction on Cu(111) is not fully understood and there are some inconsistencies in both experimental and computational results. Theoretical calculations have shown that WGS on Cu(111) proceeds either mainly through the redox mechanism [4] or a carboxyl-mediated route [7] or via both mechanisms [6]. Furthermore, computational results have shown that all three, redox, carboxyl and formate, pathways contribute similarly in the WGS reaction on Cu(111) [5]. In addition another mechanism was also proposed where CO_2 is formed from the reaction of CO with OH without forming an intermediate, however, this path and the formate (HCOO) intermediate mechanism were shown to be kinetically unlikely because of the high barrier of formation [6]. On the other hand, the carboxyl (COOH) intermediate mechanism and the redox mechanism were demonstrated to be feasible [6]. Formates (HCOO) have also been shown as a stable spectator species in the WGS process [7]. In spite of these numerous studies, open questions still remain about the reaction mechanism, key intermediates and oxidation state of the metal centers, which hinders the design and optimization of catalysts. The best way to seek answers to these questions is in situ characterization of the active state of the catalyst as close to the realistic WGS reaction conditions as possible, or as theoretically and experimentally feasible. In this study we provide new insights into the understanding of the WGS reaction mechanism on Cu(111) by investigating the interaction of H_2O and CO in situ under reaction conditions (90 mTorr CO + 30 mTorr H_2O) with ambient pressure X-ray photoelectron spectroscopy (AP-XPS).

In both redox and associative mechanisms, the rate determining step is the barrier associated with the dissociation of H_2O to form adsorbed OH and H. The fundamental reactivity of water with solid surfaces has been reviewed extensively in previous studies [8, 9]. Generally, metals surfaces have demonstrated very weak reaction with H_2O but have shown good reactivity towards CO [10–14]. However oxide surfaces behave in the opposite manner where there is poor reaction with CO but good reactivity with H_2O. We have shown previously that combining both the oxide (CeO_x) and a metal [Cu(111)] together in an inverse catalyst geometry can help to achieve a favorable response to both reactants [10]. As we will discuss below, the coupling of Cu to an oxide, Cu–CeO_2 catalyst, or a carbide, Cu–TiC catalyst, leads to a change in the reaction mechanism and produces a

very large increase in the rate for the production of H_2 through the WGS.

2 Experimental Methods

The soft X-ray photoemission measurements at UHV, presented in this manuscript were performed in situ at Beamline U12a of the National Synchrotron Light Source (NSLS) at Brookhaven National Laboratory (BNL). This beam line and UHV end station have been described in detail previously [15]. The O 1s data we report were taken at 600 eV and at a pass energy of 10 eV with an energy resolution of 0.3 eV standardized for all spectra. The spectra are all normalized to the decaying beam current to ensure correct relative intensities. The binding energy calibration was achieved using the position of the Cu Fermi edge. The commercial Cu(111) crystal was cleaned with several sequential cycles including Ar^+ sputtering (1 kV, 300 K), flash heating to 900 K and then annealing at 800 K in UHV for 20 min. Chemisorbed O was deposited on the Cu(111) surface by exposure to 10 L of O_2 at 300 K, while heavier oxidation of Cu(111) involved exposure of the sample at 650 K to 150 L of O_2. Oxidation state changes in the Cu as a result of growth of the oxide layer was monitored by examining the Cu 2p core level and Cu Auger line shapes using a $MgK\alpha$ X-ray source mounted in a separate UHV chamber located at the BNL Chemistry Department.

Infrared reflection absorption spectroscopy (IRRAS) experiments were performed in a combined UHV surface analysis chamber and elevated-pressure reactor/IRRAS cell system [16]. This system is additionally equipped with Auger electron spectroscopy (AES), low energy electron diffraction (LEED), and temperature program desorption (TPD). The elevated-pressure cell is coupled to a commercial Fourier transform infrared (FT-IR) spectrometer (Bruker, IFS 66v/S). A Cu(111) single crystal was mounted using a Ta loop embedded into a groove machined around the crystal edge. The Ta loop was attached directly to the manipulator feed-through which was used for both mechanical support and heating/cooling. The sample temperature was measured by a K-type thermocouple attached to the top edge of the crystal. The Cu(111) sample was cleaned by repeated cycles of Ar^+ sputtering and annealing to 850 K. IRRA spectra were collected at 4 cm^{-1} resolution using a grazing angle of approximately 85° to the surface normal. The chemisorbed O layer was obtained by exposing the Cu(111) to O_2 at 300 K. All of the IR spectra were referenced to a background spectrum from the sample [Cu(111), O/Cu(111), and Cu_2O/Cu(111)] prior to the CO and D_2O adsorption.

Ambient pressure XPS (AP-XPS) measurements were performed at the Advanced Light Source in Berkeley, California at beamline 9.3.2. Emitted electrons from the sample under reaction pressures and temperature were studied using a VG-Scienta R4000 HiPP analyser. Sample preparation, including $Ar+$ sputtering and annealing were performed in a separate preparation chamber attached to the reaction/analysis chamber and the beamline; all of which are described in detail elsewhere [17]. High purity gases of CO and H_2O were checked with a residual gas analyzer (RGA) mounted in the first differential stage of the analyzer and introduced onto the sample via 'backfilling' method using a set of precision leak valves attached to the reaction chamber, and traps were utilized along gas lines to prevent contaminants. Gas pressures were monitored using an ion gauge (UHV-10^{-4} Torr) and baratron gauge (10^{-4} Torr–100 mTorr) combinations. O 1s and C 1s regions were probed with photon energies of 700 and 490 eV, respectively at a pass energy of 20 eV and energy resolutions of nominally ±0.2–0.3 eV. Absolute energy calibrations were performed where possible with the Cu 2p, Cu Fermi and gas phase signals from CO and H_2O.

The WGS activity of Cu(111) was tested and compared to that of CeO_x/Cu(111) and Cu/TiC(001) surfaces. The Cu/TiC(001) and CeO_x/Cu(111) systems were prepared following the procedures described in Refs. [3, 10], respectively. The testing of catalytic activity was carried out in an UHV chamber that has attached a high-pressure cell or batch reactor [3, 10]. The sample could be transferred between the reactor and vacuum chamber without exposure to air. The UHV chamber (base pressure $\sim 5 \times 10^{-10}$ Torr) was equipped with instrumentation for XPS, LEED, ion scattering spectroscopy (ISS), and TPD. In the kinetic measurements the sample was transferred to the batch reactor at $\sim$300 K, then the reactant gases were introduced (20 Torr of CO and 10 Torr of H_2O) and the sample was rapidly heated to the reaction temperature (450–650 K). The CO gas was cleaned of any metal carbonyl impurity by passing it through purification traps. Product yields were analysed by a gas chromatograph [3, 10]. The amount of molecules produced was normalized by the active area exposed by the sample. The sample holder was passivated by extensive sulphur poisoning (exposure to H_2S) and had no catalytic activity. In our reactor a steady-state regime for the production of H_2 and CO_2 was reached after 2–3 min of reaction time. The kinetic experiments were done in the limit of low conversion (<5 %). The preparation and conditioning of substrates and reactants were carried following procedures detailed elsewhere [1, 10, 12].

3 Results and Discussion

3.1 Studies for the WGS on Cu(111)

3.1.1 Adsorption of CO on Cu(111)

First we investigated the interactions of CO on clean Cu(111) with XPS and IRRAS under UHV conditions as shown in

Fig. 2 O 1s XPS data following the adsorption of H_2O, 2 Langmuir (L) exposure, at 90 K onto *a* a clean Cu(111) sample, *b* O/Cu(111) and *c* a Cu_2O-like layer (Cu_2O/Cu(111)) and annealing to 250 K. The O/Cu(111) and Cu_2O/Cu(111) systems were prepared by exposing Cu(111) to O_2 at 300 and 650 K, respectively. *Insets* show STM images of the corresponding systems before water adsorption. STM images of Cu_2O/Cu(111) and O/Cu(111) are 10×10 nm^2; STM image of Cu(111) is 5×5 nm^2
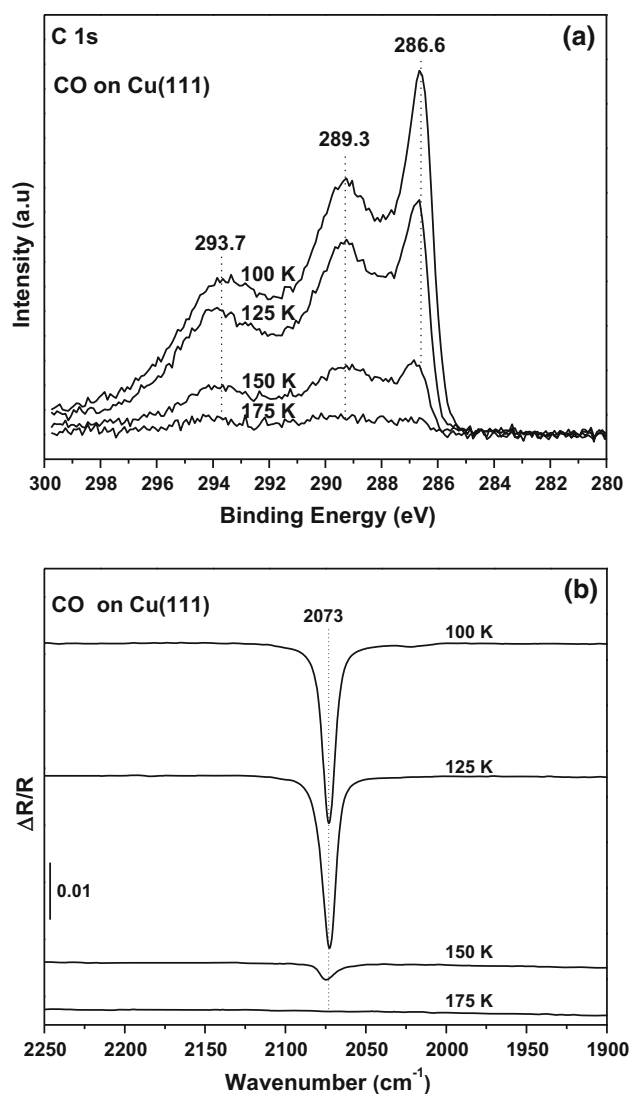
Fig. 1 **a** O 1s XPS data following the adsorption of CO at 100 K and subsequent annealing to the indicated temperatures. **b** IRRA spectra following the adsorption of CO at 100 K and subsequent annealing to the indicated temperatures

Fig. 1. Following the adsorption of CO on Cu(111) at 100 K, XPS data shows a complex spectrum with three peaks at 286.6, 289.3 and 293.7 eV. These shake up and shake off structures in XPS spectra arising from CO chemisorption on Cu surfaces have also been previously reported [18]. Intensities of these three peaks gradually decrease upon annealing to 150 K. At 175 K, all the peaks disappear completely indicating the molecular desorption of CO from the surface as shown in Fig. 1a. The IRRA spectrum shows only one peak at 2073 cm^{-1} for the linearly adsorbed CO on atop sites as shown in Fig. 1b and as reported previously [14, 15]. The intensity of this peak gradually decreases upon annealing to higher temperatures. Similar to the XPS results, the peak at 2073 cm^{-1} completely disappear after annealing to 175 K due to the desorption of CO. The data in Fig. 1 shows that CO
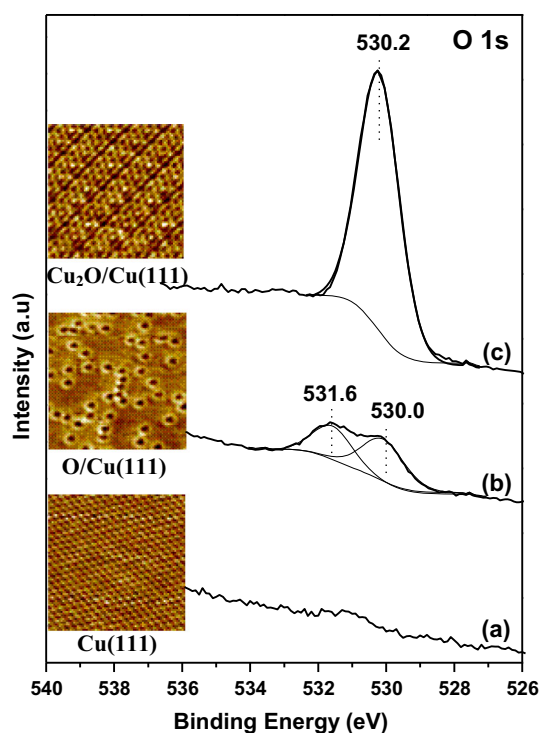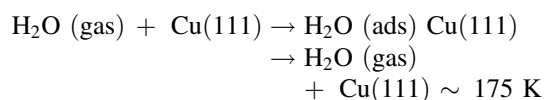
adsorbs weakly on Cu(111) and desorbs molecularly upon annealing to 175 K. This is in agreement with previous studies for CO adsorption on Cu(111) [14, 15]. Thus, CO does not stay bound to the copper surface at the typical WGS reaction temperatures ($\sim$450–600 K).

3.1.2 Reaction of H_2O with Cu(111), Cu_2O/Cu(111) and O/Cu(111) Surfaces

We investigated the interactions of H_2O on clean Cu(111), O/Cu(111), and Cu_2O/Cu(111) surfaces under UHV conditions. Figure 2 depicts the O 1s spectra obtained following annealing of the H_2O-adsorbed systems, 2 Langmuir (L) at 90–250 K. After annealing of H_2O-adsorbed Cu(111) to 250 K, no O 1s peak was observed as shown by Fig. 2a indicating the desorption of molecular H_2O without dissociation.

$$H_2O \text{ (gas)} + \text{Cu(111)} \rightarrow H_2O \text{ (ads) Cu(111)}$$
$$\rightarrow H_2O \text{ (gas)}$$
$$+ \text{Cu(111)} \sim 175 \text{ K}$$

There is no OH species and no evidence of the dissociation of H_2O from this atomically flat Cu(111) surface
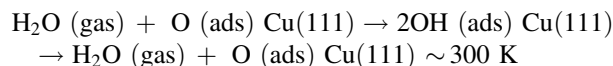
(see inset STM image in Fig. 2a) under the UHV conditions. It has been reported using Ambient pressure XPS experiments at 1 Torr of H_2O at 300 K, that the Cu(111) surface failed to dissociate water [12]. Figure 2c shows the results obtained from the Cu_2O/Cu(111) system. The atomistic structure of this Cu_2O-like layer (see inset STM image Fig. 2c) is the focus of STM studies reported elsewhere [19]. After annealing to 250 K, all the ice layers have desorbed from Cu_2O/Cu(111) leaving a peak at 530.2 eV, which is similar to the feature for the initial Cu_2O-like oxide layer before exposure to H_2O. Thus, there is no OH species and no evidence of the dissociation of H_2O from the Cu_2O/Cu(111) surface under the UHV conditions. This implies that the Cu_2O surface does not have the ability to dissociate H_2O and the adsorption and desorption follows a weak interaction.

$$H_2O \ (gas) \ + \ O \ (Cu_2O) \rightarrow H_2O \ (ads) \ O(Cu_2O)$$
$$\rightarrow H_2O \ (gas)$$
$$+ \ O(Cu_2O) \sim 175 \ K$$
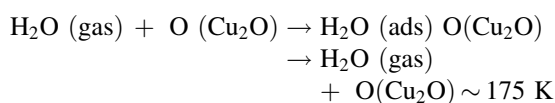
Following annealing of the H_2O-adsorbed O/Cu(111) to 250 K, two peaks appear at ∼530.0 and ∼531.6 eV in the O 1s spectrum as shown in Fig. 2b. The peak at ∼530.0 can be assigned to a fraction of chemisorbed O remaining on the surface whereas the peak at 531.6 eV is for OH species indicating the dissociation of H_2O on the chemisorbed O layer. A detailed description of the dissociation of H_2O on O/Cu(111) is shown by Fig. 3.

Figure 3 shows the O 1s XPS data of H_2O (2 Langmuir exposure) interactions at 90 K with chemisorbed O (∼0.1 ML) on the Cu(111) surface. The bottom spectrum in Fig. 3, which shows a peak at 529.5 eV, is for the chemisorbed O layer (O/Cu(111)) before exposure to H_2O. After exposing O/Cu(111) to H_2O at 90 K, a peak at 533.9 eV appears for multilayers of H_2O (ice) with a broad yet weak shoulder at ∼531.4 eV. As in the case of the clean Cu(111) surface (data not shown) no visible changes are obvious from 90 to 120 K with the multilayer ice structures remaining uniform in chemical composition. At 150 K there is an abrupt decomposition as the ice layers melt, with a more pronounced peak at 531.4 eV. At 175 K, the ice layers (533.9 eV) has desorbed completely leaving the most predominant peak at 531.4 eV, which can be assigned to OH derived from the dissociation of O–H bonds in H_2O [20, 21]. The peak area of the 531.4 eV peak is approximately two times larger than that of the peak at 529.5 eV, which is attributed to the initial amount of chemisorbed O, indicating that the dissociation of each H_2O molecule on O forms two hydroxyls. From 175–250 K, there is a gradual decrease of the OH peak with desorption of H_2O occurring until 300 K where all that is left is a small amount of O with a peak at 529.5 eV in equal concentration to the initial amount of chemisorbed

O. This result signifies that the chemisorbed O is able to activate the dissociation of H_2O on the Cu(111) surface to form OH but the O does not prevent the desorption of H_2O through recombination of OH groups (see below), which eliminates the pathway for the production of H_2 through the dissociation of OH.

$$H_2O \ (gas) \ + \ O \ (ads) \ Cu(111) \rightarrow 2OH \ (ads) \ Cu(111)$$
$$\rightarrow H_2O \ (gas) \ + \ O \ (ads) \ Cu(111) \sim 300 \ K$$

We have also investigated the interaction of water (D_2O) on clean Cu(111), Cu_2O/Cu(111) and O/Cu(111) with IRRAS. Figure 4 shows the IRRA spectra obtained following the exposure of O/Cu(111) to D_2O at 160 K and subsequent annealing to the specified temperatures. Following the exposure of O/Cu(111) to D_2O at 160 K, a peak appears at 2690 cm^{-1}, which can be assigned to the O-D stretch, ν(O-D), of the hydroxyl (OD) group. The intensity of this peak gradually decreases and slightly shifts (due to coverage effects) after annealing above 200 K, disappearing completely at 275 K. This data is in close correlation to the XPS results and indicates that D_2O dissociates at 160 K on O/Cu(111) to form OD, which desorb as D_2O as shown by the data in Fig. 3. Similar results were observed following the adsorption of multilayers D_2O at 100 K and subsequent annealing to higher temperatures. The IR peak for ν(O-D) of hydroxyl group was not observed following the adsorption of D_2O on Cu(111) or Cu_2O/Cu(111), spectra not shown. This is similar to the results observed in the XPS experiments confirming that Cu(111) and Cu_2O/Cu(111) do not have ability to dissociate water.

3.1.3 Interactions of OH with CO on Cu(111)

Figure 5a, b show the IRRA spectra obtained following the co-adsorption of CO on the OD layer at 120 K and subsequent annealing to the specified temperatures, respectively. The top spectrum in Fig. 5a is for the hydroxyl layer prepared by adsorbing D_2O at 160 K on O/Cu(111) and the other spectra are for the co-adsorption of CO as a function of CO coverage (the sample was cool down in the presence of 1×10^{-7} Torr of CO). At the lowest CO coverage, a weak broad feature centered at 2067 cm^{-1} appears for co-adsorbed CO. With increasing CO coverage, the peak for CO at 2067 cm^{-1} grows and simultaneously intensity of the OD peak at 2689 cm^{-1} gradually decreases and finally the OD peak disappears completely as shown by the bottom spectrum in Fig. 5a. The IRRA spectra obtained following annealing of the co-adsorbed CO + OD layer is shown in Fig. 5b. The lowest spectrum of Fig. 5b is same result as the lowest spectrum of Fig. 5a. After annealing of co-adsorbed CO + OD layer to 140 K, the intensity of the CO peak at 2067 cm^{-1} decreases due to the desorption of CO and simultaneously a weak feature for OD appears at
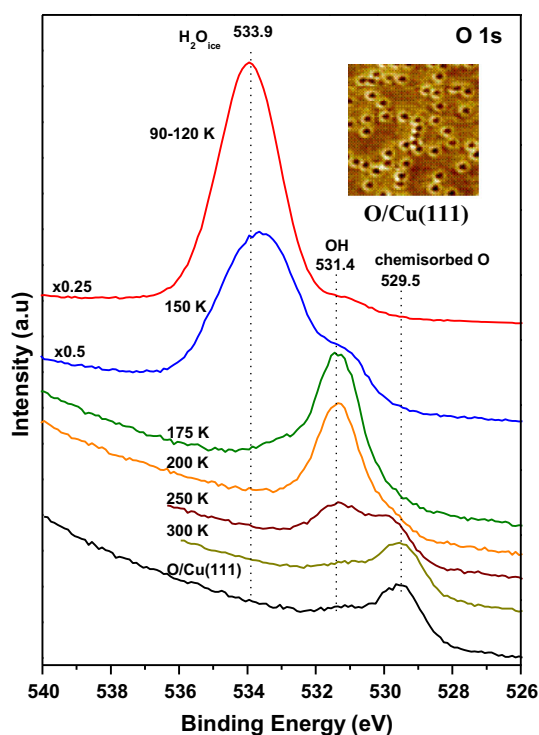
Fig. 3 O 1s XPS data following the adsorption of H$_2$O, 2 Langmuir (L) exposure, onto a chemisorbed O layer on Cu(111) (O/Cu(111)) at 90 K and subsequent annealing to the specified temperatures. The O/Cu(111) system was prepared by dosing 10 L of O$_2$ at 300 K. *Inset* show STM image of the corresponding system before water adsorption
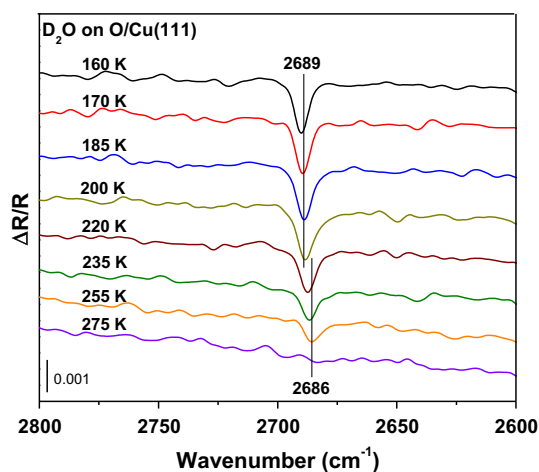

Fig. 4 IRRA spectra obtained following the exposure of O/Cu(111) to D$_2$O at 160 K and subsequent annealing to the specified temperatures. The O/Cu(111) system was prepared by dosing 100 L of O$_2$ at 300 K

2689 cm^{-1}. The peak at 2067 cm^{-1} completely disappears upon annealing to 150 K, and the intensity of the OD peak increases. Further annealing above 200 K leads to the intensity decrease of the peak at 2689 cm^{-1} and the OD peak completely disappears at 275 K, similar to the OD layer on
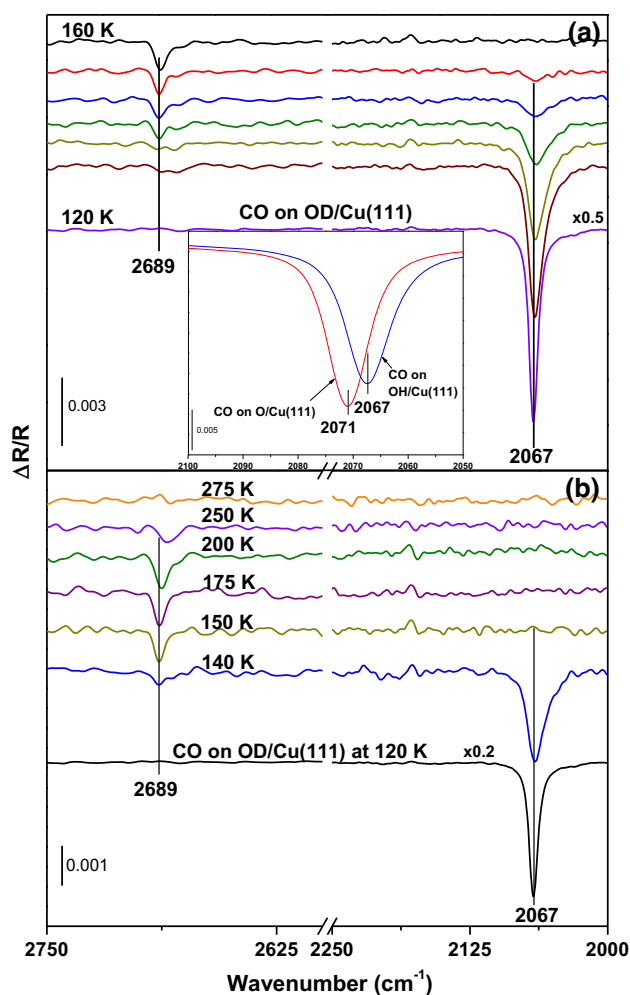

Fig. 5 IRRA spectra obtained following **a** co-adsorption of CO on the OD layer at 120 K and **b** subsequent annealing to the specified temperatures. The OD layer was prepared by following the exposure of O/Cu(111) to D$_2$O at 160 K

Cu(111) without co-adsorbed CO as shown in Fig. 4. The IR peak for co-adsorbed CO with OD appears at 2067 cm^{-1} whereas the peak for co-adsorbed CO with chemisorbed O is at 2071 cm^{-1}, which is very similar to the IR peak for CO on clean Cu(111), as shown by the inset in Fig. 5a. This frequency shift of the peak for co-adsorbed CO with OD indicates the interaction between OD and CO, which also causes the disappearance of the OD peak in the spectrum. Most likely, the interaction between CO and OD causes a tilt to the upright OD species to a more parallel orientation with respect to the surface, which leads to the disappearance of the OD peak in the IRRA spectrum according to the metal surface selection rules [22]. This data also indicates that even though the co-adsorbed CO and OD interact they do not react associatively to form any "COOD" like intermediates, but instead they just desorb from the surface under the conditions applied in this study. Similar results were observed in XPS experiments (data not

shown). Even though we do not observe a stable "COOD" like intermediate under UHV conditions it is possible to form such intermediates on Cu(111) under WGS reaction conditions. Therefore, the interaction of H_2O with CO was investigated under WGS reaction conditions using ambient pressure XPS (AP-XPS) and results are discussed in the following section.

3.1.4 Interactions of H_2O + CO on Cu(111) at Ambient Pressures

Figure 6a, b show the O and C 1s regions, respectively, upon in situ interactions of H_2O + CO on clean Cu(111). At total pressures of 120 m Torr (90 mTorr of CO and 30 mTorr of H_2O), the O 1s spectrum shows features for gas phase CO and H_2O and peaks at 533.0 and 531.6 eV for surface species. The feature at 531.6 eV can be assigned to OH species derived from the dissociation of H_2O. The C 1s spectrum shows peaks at 284.8 and 286.5 eV with a broad feature at 287.0–291.0 eV for surface species in addition to the gas phase CO. A peak at 533.0 eV in the O 1s and a peak in the C 1s at 286.5 can be assigned to the chemisorbed CO onto the Cu(111) surface as reported previously [18] and as shown in Fig. 1a. The feature at 284.8 eV in the C 1s spectrum is due to hydrocarbon contaminants. No indication of the presence of chemisorbed O species is observed at ~529.5 eV in Fig. 3. This indicates that as soon as O species form from the dissociation of water they react with CO to produce CO_2. No other features are observed for the surface species on the Cu(111) surface at 473 K due to the interaction between CO + H_2O. Similar results were also observed at 573 K. However, previous studies have shown that the WGS is active to produce H_2 on Cu(111) under these conditions (bottom of Fig. 7) [10]. Since the intermediate species other than CO and OH are not observed on Cu(111) under reaction conditions, we propose that the WGS reaction can take place predominantly via a redox mechanism on Cu(111) rather than via an associative mechanism through "OHCO" like species. However, we cannot completely rule out the presence of another minor pathway for WGS via the associative mechanism on Cu(111) simply due to the fact that there is an inability to detect certain intermediate species. Furthermore, if only weak features are present for the intermediate species they may be masked by the strong peaks for CO and OH in the XP spectra. In addition, the WGS can take place via another pathway, in which CO and OH interact to produce H_2 without forming an intermediate as predicted by theoretical calculations [6]. However, this path has been shown to be kinetically unlikely because of the high formation barrier. Based on the above reasons, most likely, the redox mechanism is the dominant WGS
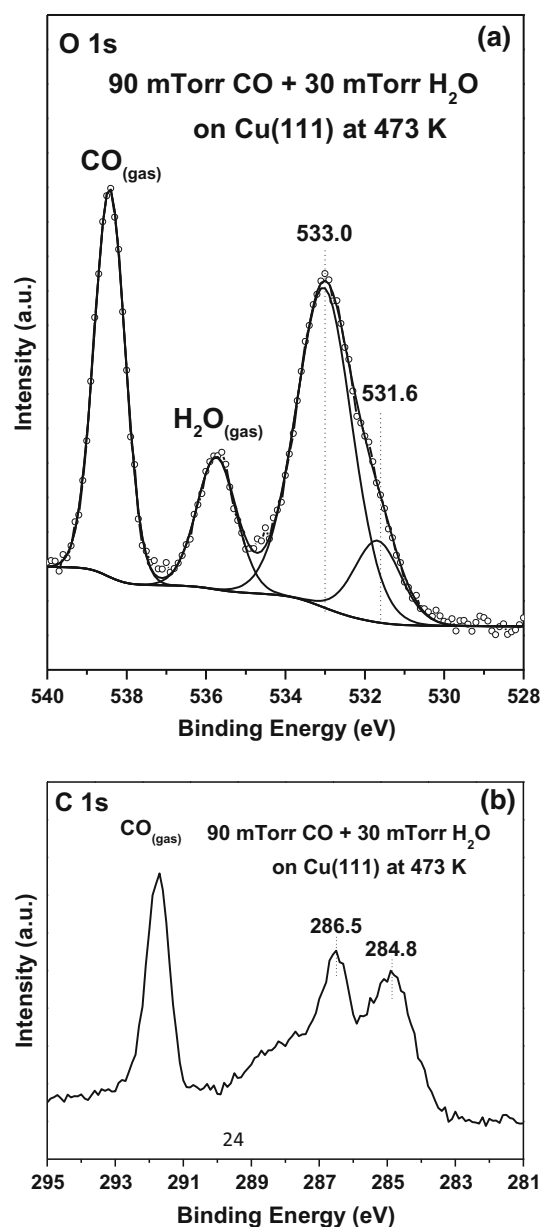

Fig. 6 Ambient pressure XPS data in **a** O 1s and **b** C 1s regions under WGS reaction conditions (90 mTorr CO + 30 mTorr H_2O) on Cu(111) at 473 K. Experimental data for O 1s is shown by a *line with open circles* whereas the *solid lines* are for peak fitting results

pathway on Cu(111) under the conditions applied in this study.

3.2 Studies for the WGS on CeO$_x$/Cu(111)

3.2.1 WGS Activity of Cu(111) Versus CeO$_x$/Cu(111)

Figure 7 displays the WGS activity of Cu(111) after covering ~20 % of this surface with ceria islands. The CeO$_x$ nanoparticles supported on Cu(111) generated a catalyst that was eight-times (at 650 K) to 23-times (at 575 K)
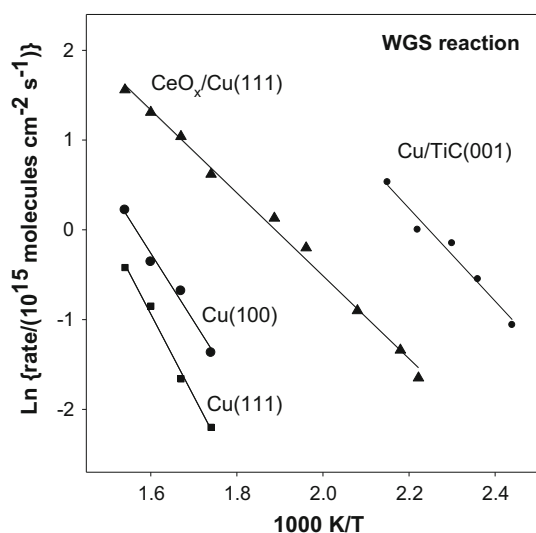
Fig. 7 Arrhenius plots for the WGS on Cu(111), Cu(100), CeO$_x$/Cu(111) and Cu/TiC(001). The Cu coverage on TiC(001) was ~0.2 ML. P_{CO} = 20 Torr, P_{H_2O} = 10 Torr

Fig. 8 0041P-XPS spectra of Cu(111) and CeOx/Cu(111) under WGS reaction conditions (Reproduced with permission from ref. 23, Copyright © 2013 WILEY-VCH Verlag GmbH & Co. KGaA, Weinheim)

more active than the clean Cu(111) substrate. The data in Fig. 7 for CeO$_x$/Cu(111) were collected at temperatures between 450 and 650 K. From the Arrhenius graph in Fig. 7, one can determine an apparent activation energy of 18 kcal/mol for the WGS on Cu(111), which is 2–5 kcal/mol larger than those found on Cu(100) and Cu(110) [1]. In contrast the apparent activation energy for the WGS on CeO$_x$/Cu(111) is only 9 kcal/mol. This value is close to that found for Cu/CeO$_2$(111) and smaller than the value of 13 kcal/mol found for Cu nanoparticles supported on ZnO(000ī) [10]. Under WGS conditions, most of the cerium in CeO$_x$/Cu(111) is a +3 oxidation state and has no problem dissociating water [10]. The OH groups formed by the dissociation of water react with CO at the copper-ceria interface [23].

3.2.2 Interaction Between OH and CO on CeO$_x$/Cu(111)

We have previously reported AP-XPS experiments examining species adsorbed on the CeO$_x$/Cu(111) catalyst under WGS reaction conditions [23]. Figure 8 shows the corresponding AP-XPS spectra [from Ref. 23] obtained during the WGS reaction on CeO$_x$/Cu(111), where the comparison with the same conditions on plain Cu(111), as shown in Fig. 6, is also included in Fig. 8a. A very different picture emerges on CeO$_x$/Cu(111). In the O 1s region, the peak at 530.0 eV in Fig. 8b is associated with oxygen from the CeO$_x$ nanoparticles [23]. The feature at 531.8 eV is related to OH groups, and the shoulder at a higher binding energy is due to the adsorption of CO [23]. Increasing the temperature brings several changes (Fig. 8c and d). The features due to chemisorbed CO and OH decreased in intensity or disappeared, and a new peak in the O 1s region
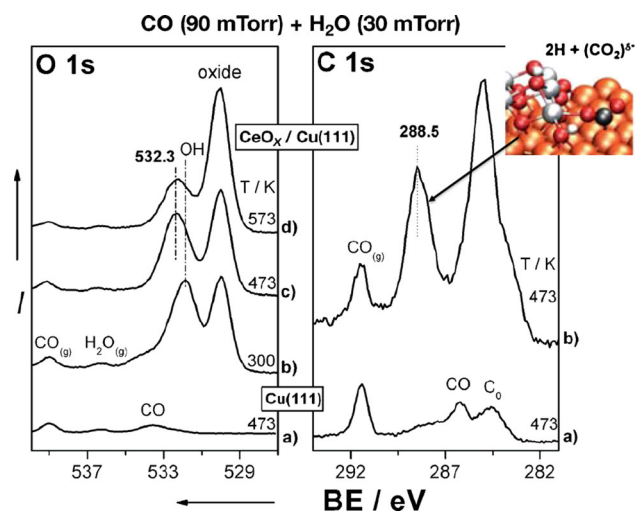
at 532.3 eV develops. This could be related to many different surface species. In the C 1s region (Fig. 8b) two peaks at 288.5 and 285 eV develop. The peak at 285 eV is associated to C$_0$. The peak at 288.5 eV, similar to the peak at 532.3 eV in the O 1s region, can be associated to various species. Based on control experiments and comparison with related reports in the literature, it was concluded that the most abundant species under WGS conditions on CeO$_x$/Cu(111) were carboxylates. The presence of a CO$_2^{\delta-}$ species is consistent with studies of IR spectroscopy and DFT calculations [23]. The theoretical calculations indicate that the CO$_2^{\delta-}$ is a consequence of the decomposition of a COOH intermediate formed by the reaction of OH and CO at the ceria-copper interface [23]. Since the CO$_2^{\delta-}$ species is not observe on either CeO$_2$ films or clean Cu(111) [23], the interfacial sites formed on the CeO$_x$/Cu(111) system appear to be critical for the formation and stabilization of CO$_2^{\delta-}$. Thus, the existence of these sites opens the route for an associative pathway and high activity for the WGS reaction.

3.3 Studies for the WGS on Cu/TiC(001)

3.3.1 Electronic Perturbations on Cu and Decomposition of H$_2$O on Cu/TiC(001)

In the previous section we found an enhancement in catalytic activity when copper was coupled to ceria in a metal-oxide interface. The oxide helped with the dissociation of water providing OH groups that could react with the CO bound to copper. An alternative approach to enhance the chemical activity of Cu involves the deposition of this
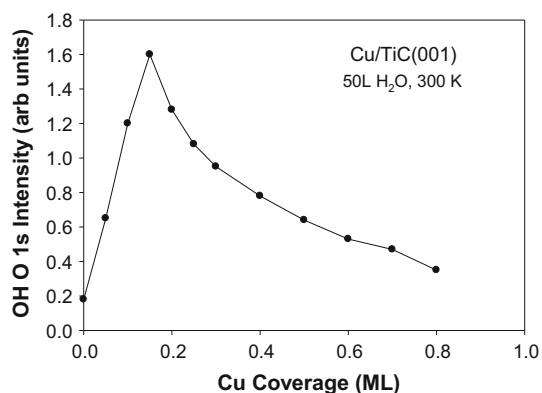
Fig. 9 O 1s XPS intensity for the OH peak obtained after dosing 50 L of water at 300 K to a series of Cu/TiC(001) surfaces with different copper coverages

metal on carbide substrates [24, 25]. For example, Cu atoms in contact with TiC(001) undergo a charge polarization that makes them more reactive than the atoms in Cu(111) [24, 25]. As mentioned above, Cu(111) does not dissociate water at 300 K [12]. In XPS experiments for the partial dissociation of water on Cu/TiC(001) ($H_2O \rightarrow OH + H$), we found high reactivity for surfaces that had a copper coverage below 0.2 ML (see Fig. 9). At coverages above 0.2 ML, the Cu formed predominantly three-dimensional (3D) particles on TiC(001) [24, 25]. This minimized the effects of Cu $\leftrightarrow$ TiC interactions with a drop in chemical activity. Upon the dissociative adsorption of water on Cu/TiC(001) systems ($\Theta_{Cu} < 0.2$ ML), we observed a relatively narrow Cu $2p_{3/2}$ peak in the XPS spectrum, with a binding energy shift of 0.8–1.0 eV with respect to clean Cu/TiC(001), which is consistent with the formation of $Cu(OH)_x$ compounds. These compounds can play an active role in the WGS process [3].

3.3.2 WGS Activity of Cu/TiC(001) Versus Cu(111) and CeO$_x$/Cu(111)

Figure 7 compares the WGS activities of Cu(111), Cu(100), CeO$_x$/Cu(111) and a TiC(001) surface pre-covered with ~0.2 ML of Cu. At relatively low temperatures (<470 K), Cu/TiC(001) exhibits a WGS activity that is observed on copper surfaces and on Cu-oxide surfaces only at elevated temperatures (>500 K). The apparent activation energy for the process decreases from 18 kcal/mol on Cu(111) to 9 kcal/mol on CeO$_x$/Cu(111) and 10 kcal/mol on Cu/TiC(001). Two important issues when dealing with the use of metal carbides as possible catalysts for the water–gas shift are selectivity and stability [26]. In our studies for the WGS reaction on Cu/TiC(001), the only products detected were H_2 and CO_2 (i.e. no methane). On the other hand at the relatively low temperatures used for the experiments with Cu/TiC(001), <470 K, the water did not

attack the TiC to form an oxycarbide. After 6 h of catalytic testing, we did not observe any signs for deactivation of the Cu/TiC(001) catalyst. Preliminary studies with DFT indicate that the mechanism for the WGS on Cu/TiC(001) follows an associative pathway with COOH as a key intermediate. This intermediate has also been observed in studies for the reverse WGS [25].

4 Conclusions

The Cu(111) and Cu$_2$O/Cu(111) surfaces are not active for the dissociation of water under UHV conditions. Whereas, H_2O did readily dissociate on a chemisorbed O layer on Cu(111) to form OH species. Even though this OH interacts with adsorbed CO, it does not react to form a "OHCO" like intermediate and desorbs as H_2O at 275 K without producing H_2 under UHV conditions. Even under WGS reaction conditions no intermediates except CO and OH were observed in the reaction of CO with H_2O although the catalytic production of H_2 occurred under these conditions. Since intermediate species other than CO and OH were not observed on Cu(111) under reaction conditions, we concluded that most likely, the redox mechanism is the dominant WGS pathway on Cu(111) although we cannot completely rule out the presence of another minor pathway via the associative mechanism. Routes for an associative mechanism, via a COOH intermediate, are opened after forming Cu-ceria and Cu–TiC interfaces. On these interfaces the WGS takes place at much faster rates than on pure metallic copper.

References

1. Nakamura J, Campbell JM, Campbell CT (1990) Kinetics and mechanism of the water-gas shift reaction catalysed by the clean and Cs-promoted Cu(110) surface: a comparison with Cu(111). J Chem Soc, Faraday Trans 86(15):2725–2734
2. Oyama T (ed) (1996) Chemistry of metal carbides and nitrides. Springer, Berlin, p 536
3. Rodriguez JA, Ramirez PJ, Asara GG, Viñes F, Evans J, Liu P, Ricart JM, Illas F (2014) Charge polarization at a Au-TiC interface and the generation of highly active and selective catalysts for the low-temperature water-gas shift reaction. Angew Chem Int Ed 53(42):11270–11274. doi:10.1002/anie.201407208
4. Jakdetchai O, Nakajima T (2002) Mechanism of the water–gas shift reaction over Cu(110), Cu(111) and Cu(100) surfaces: an AM1-d study. J Mol Struc-Theochem 619(1–3):51–58

5. Lin C-H, Chen C-L, Wang J-H (2011) Mechanistic studies of water–gas-shift reaction on transition metals. J Phys Chem C 115(38):18582–18588

6. Tang Q-L, Chen Z-X, He X (2009) A theoretical study of the water gas shift reaction mechanism on Cu(111) model system. Surf Sci 603(13):2138–2144

7. Gokhale AA, Dumesic JA, Mavrikakis M (2008) On the mechanism of low-temperature water gas shift reaction on copper. J Am Chem Soc 130(4):1402–1414

8. Henderson MA (2002) The interaction of water with solid surfaces: fundamental aspects revisited. Surf Sci Rep 46(1–8):1–308

9. Thiel PA, Madey TE (1987) The interaction of water with solid surfaces: fundamental aspects. Surf Sci Rep 7(6–8):211–385

10. Rodriguez JA, Graciani J, Evans J, Park JB, Yang F, Stacchiola D, Senanayake SD, Ma S, Pérez M, Liu P, Sanz JF, Hrbek J (2009) Water-gas shift reaction on a highly active inverse CeOx/Cu(111) catalyst: unique role of ceria nanoparticles. Angew Chem Int Ed 48(43):8047–8050

11. Hinch BJ, Dubois LH (1992) Stable and metastable phases of water adsorbed on Cu(111). J Chem Phys 96(4):3262–3268

12. Yamamoto S, Andersson K, Bluhm H, Ketteler G, Starr DE, Schiros T, Ogasawara H, Pettersson LGM, Salmeron M, Nilsson A (2007) Hydroxyl-induced wetting of metals by water at near-ambient conditions. J Phys Chem C 111(22):7848–7850

13. Wang G-C, Nakamura J (2010) Structure sensitivity for forward and reverse water-gas shift reactions on copper surfaces: a DFT study. J Phy Chem Lett 1(20):3053–3057

14. Hollins P, Pritchard J (1979) Interactions of CO molecules adsorbed on Cu(111). Surf Sci 89(1–3):486–495

15. Senanayake SD, Mullins DR (2008) Redox pathways for HCOOH decomposition over CeO2 surfaces. J Phys Chem C 112(26):9744–9752

16. Hrbek J, Hoffmann FM, Park JB, Liu P, Stacchiola D, Hoo YS, Ma S, Nambu A, Rodriguez JA, White MG (2008) Adsorbate-driven morphological changes of a gold surface at low temperatures. J Am Chem Soc 130(51):17272–17273

17. Grass ME, Karlsson PG, Aksoy F, Lundqvist M, Wannberg B, Mun BS, Hussain Z, Liu Z (2010) New ambient pressure photoemission endstation at advanced light source beamline 9.3.2. Rev Sci Instrum 81(5):053106. doi:10.1063/1.3427218

18. Tillborg H, Nilsson A, Mårtensson N (1993) Shake-up and shake-off structures in core level photoemission spectra from adsorbates. J Electron Spectrosc Relat Phenom 62(1–2):73–93

19. Yang F, Choi Y, Liu P, Hrbek J, Rodriguez JA (2010) Autocatalytic reduction of a Cu2O/Cu(111) surface by CO: sTM, XPS, and DFT studies. J Phys Chem C 114(40):17042–17050

20. Senanayake SD, Stacchiola D, Evans J, Estrella M, Barrio L, Pérez M, Hrbek J, Rodriguez JA (2010) Probing the reaction intermediates for the water–gas shift over inverse CeOx/Au(111) catalysts. J Catal 271(2):392–400

21. Senanayake SD, Waterhouse GIN, Chan ASY, Madey TE, Mullins DR, Idriss H (2007) The reactions of water vapour on the surfaces of stoichiometric and reduced uranium dioxide: a high resolution XPS study. Catal Today 120(2):151–157

22. Hoffmann FM (1983) Infrared reflection-absorption spectroscopy of adsorbed molecules. Surf Sci Rep 3(2–3):107–192

23. Mudiyanselage K, Senanayake SD, Feria L et al (2013) Importance of the metal-oxide interface in catalysis: in situ studies of the water-gas shift reaction by ambient-pressure X-ray photoelectron spectroscopy. Angew Chem Int Ed 52:5101–5105

24. Rodriguez JA, Illas F (2012) Activation of noble metals on metal-carbide surfaces: novel catalysts for CO oxidation, desulfurization and hydrogenation reactions. Phys Chem Chem Phys 14:427–438

25. Rodriguez JA, Evans J, Feria L, Vidal AB, Liu P, Nakamura K, Illas F (2013) CO2 hydrogenation on Au/TiC, Cu/TiC and Ni/TiC: production of CO, methane and methanol. J Catal 307:162–169

26. Moon DJ, Ryu JW (2004) Molybdenum carbide water-gas shift catalyst for fuel cell-powered vehicles applications. Catal Lett 92(1–2):17–24